73rd International Astronautical Congress, Paris, France, 18-22 September 2022.

IAC–22–C1.IP.37.x69012

Families of Displaced non-Keplerian Polar Orbits for Space-Based Solar Energy Applications

Onur Çelik, Colin R. McInnes
Space and Exploration Technology Group, James Watt School of Engineering, University of Glasgow, Glasgow G12 8QQ, Scotland, United Kingdom

Orbiting Solar Reflectors (OSRs) can be used to reflect sunlight locally to terrestrial solar power plants to enhance solar energy generation. Displaced polar orbits can, in principle, change the geometry of passes of OSR over terrestrial solar power plants. Such non-Keplerian orbits can be obtained by orienting the reflector at a fixed pitch angle with respect to the Sun-line, such that the solar radiation pressure (SRP) induced force would shift the orbit plane in the anti-Sun line. This, in principle, would allow extending night-time or high-latitude solar energy delivery without eclipses. This paper investigates a range of displaced highly non-Keplerian orbits for OSRs and assesses their operational use. Displaced polar orbits are generated in the two-body problem using a rotating reference frame considering the Earth's oblateness up to J_2 and the SRP force. Their stability is reviewed and an optimal control scheme is presented with reflector area control. As a novel application, a compound reflector system is proposed, which consists of a large Sun-facing parabolic collector in a polar orbit displaced in the anti-Sun direction and a smaller free-flying flat director placed near the focus of the parabolic collector, displaced by the reflected SRP in the Sun direction. The conditions for the synchronized motion and the sizing of the reflectors are investigated. The quantity of solar energy delivered to the Earth is calculated for both the compound and single reflector systems and it is shown that the displaced polar orbits could enhance solar energy delivery significantly.

1. Introduction

Orbiting solar reflectors (OSRs) can be used to reflect incoming sunlight to the Earth's surface. They were considered even before the modern space era [1] and attracted interest throughout the 20th and the 21st-century [2] for a variety of applications, including, but not limited to, space-based solar energy, nighttime illumination and agriculture [3, 4, 5, 6, 7]. Recent studies demonstrate that the concept of orbiting solar reflectors can be an asset to address the challenges associated with global energy delivery [7, 8, 9, 10, 11] and may be considered for non-terrestrial endeavours, as well [12, 13, 8].

Orbiting solar reflectors are generally made of thin, ultralight and high-reflectivity materials. This means that solar radiation pressure (SRP) could induce a force on the reflector which may be used for generating new families of non-Keplerian orbits. One such family of orbits is the so-called displaced non-Keplerian orbits (NKOs) [14]. Among these families of orbits, there is a subset of circular polar orbits along the terminator line of the Earth (or any other planetary body) displaced in the anti-Sun direction by the SRP-induced force [15]. Such orbits can be realised by keeping a fixed pitch angle attitude with respect to the Sun [15]. Indeed, displaced NKOs are, in principle, the same family of orbits as so-called terminator orbits, which are primarily termed for displaced polar orbits around asteroids, where the asteroidal gravity and SRP forces are comparable in magnitude [16], and are already employed in space missions such as OSIRIS-REx and planned for one of the CubeSats onboard ESA's HERA mission [17, 18]. The planetary applications of displaced NKOs include speculative applications for Earth and Mars climate interventions [19, 20] and Earth's geomagnetic tail exploration [21].

Displaced NKOs may also be considered for space-based solar energy applications. The primary advantage of displaced NKOs for such applications is that they are eclipse-free by definition, which would allow nighttime only energy delivery. In comparison, a Keplerian polar orbit may be tilted in its right ascension of the ascending node towards the Earth's nighttime, but this would only allow for half of the orbit to be useful for nighttime energy delivery while in the rest would be on the day side. There would also be limits before the reflector goes into the Earth's eclipse cone. Large displacements may also allow high-latitude solar energy delivery, as well, but those will require high SRP accelerations which will be achievable only with

ultra-lightweight materials.

Alternatively, as a novel application, solar energy delivery may be enhanced by using a compound reflector system. Such a system may consist of a parabolic reflector displaced in the anti-Sun direction and focusing the intercepted sunlight onto a smaller flat reflector, displacing it in the Sun direction*. The primary advantage of the compound system is the separation of focusing and directing functionalities, which are challenging for a standalone parabolic system that is both Sun- and Earth-facing and performs attitude control over a ground target. By using a compound system, the quantity of energy delivered to a solar power plant may be higher, or at least similar to that from (near-)polar orbits from higher altitudes, which may ease the requirements on the size of reflectors [8, 10]. The compound reflector discussed here is conceptually similar to solar photon thruster (SPT) [22], particularly to so-called simple SPT [22, 23]. Some other variants of SPT are also considered for GEO illumination-type application [24]. The difference between SPT and the compound concept proposed here is that two reflectors (and an additional director, where applicable) are connected by a boom and the distance between them is relatively short, whereas the proposed compound system here is two different reflector spacecraft in synchronised motion, displaced in each side of the terminator line. Even though the concept of SPT is deemed to be potentially inferior to single reflector systems in terms of thrust performance [25], the added focusing functionality could potentially be useful to increase the solar power density on the ground for space-based solar energy applications for the Earth.

In this paper, therefore, displaced non-Keplerian orbits are investigated for space-based solar energy applications. A review of non-Keplerian orbits is provided in [14]. The orbits are generated in the two-body dynamics enhanced by the Earth's oblateness up to the second order (i.e., J_2) and the SRP force in a rotating reference frame. The equilibrium conditions and stability aspects of displaced NKOs were reviewed, following the results in Ref. [20]. In this paper, controllability of displaced NKOs is investigated in addition and an optimal linear control scheme by reflector area control is presented for the unstable family of orbits in this higher fidelity dynamics. For the novel application of compound reflectors, the conditions for the synchronised motion are presented and a procedure is proposed to size the reflectors to achieve such motion. Finally, the quantity of energy delivered is calculated for both single and compound reflector systems, and the results are presented together with a comparative discussion between Keplerian and displaced non-Keplerian orbits in terms of solar energy delivery.

The paper is organised as follows: Sec. II provides a discussion on the dynamics and equilibrium conditions of displaced NKOs. Single reflectors in displaced orbits are discussed in Sec. III, including their stability and control and energy delivery properties. The proposed compound system is discussed in Sec. IV and, finally, conclusions are presented in Sec. V.

2. Dynamics of Displaced non-Keplerian Orbits

A rotating reference frame will first be defined before deriving the equations of motion of displaced non-Keplerian orbits (NKOs) [14]. This rotating reference frame has its origin coinciding with the Earth's center, with the axis of rotation, z, is parallel to the assumed fixed Earth-Sun line but pointing in the anti-Sun direction, the y-axis is parallel to the Earth's rotation axis and the x-axis completes the triad. The reflector will be considered at a distance $\mathbf{r}$ from the origin of this frame. The reflector normal can also be defined as $\mathbf{n} = \begin{bmatrix} 0 & \sin\psi & \cos\psi \end{bmatrix}^T$. Figure 1 depicts this rotating reference frame. The motion of a particle in the Earth's gravitational potential with solar radiation pressure (SRP) acceleration can be expressed with respect to the defined rotational reference frame as

$$\ddot{\mathbf{r}} + 2\boldsymbol{\omega} \times \dot{\mathbf{r}} + \boldsymbol{\omega} \times (\boldsymbol{\omega} \times \mathbf{r}) = \mathbf{a}_{\text{srp}} - \nabla V \tag{1}$$

where $\mathbf{r}$ denotes the particle's position vector from the center of the Earth, $\boldsymbol{\omega}$ denotes the angular velocity. Moreover, $\mathbf{a}_{\text{srp}}$ and V are the SRP acceleration and gravitational potential expanded by the Earth's oblateness up to the second degree as

$$V = -\frac{\mu}{r}\left(1 - \frac{3}{2}J_2\left(\frac{R_E}{r}\right)^2\left(\left(\frac{y}{r}\right)^2 - 1\right)\right) \tag{2a}$$

$$\mathbf{a}_{\text{srp}} = \kappa\cos^2\psi\begin{bmatrix} 0 & \sin\psi & \cos\psi \end{bmatrix}^T \tag{2b}$$

where μ is the Earth's gravitational parameter and equal to $398\,000 \times 10^5\,\text{km}^3\,\text{s}^{-2}$, r is the magnitude of the position vector and J_2 is the second degree zonal harmonic, whose value is equal to 1.082×10^{-3}[26]. In

*Another alternative concept with Fresnel lenses can be found at `https://ideas.esa.int/servlet/hype/IMT?documentTableId=45087132021033175&userAction=Browse&templateName=&documentId=cfab82be9ca4f4d9a2ccd0ad7aa328e0` (Accessed on August 27, 2022)

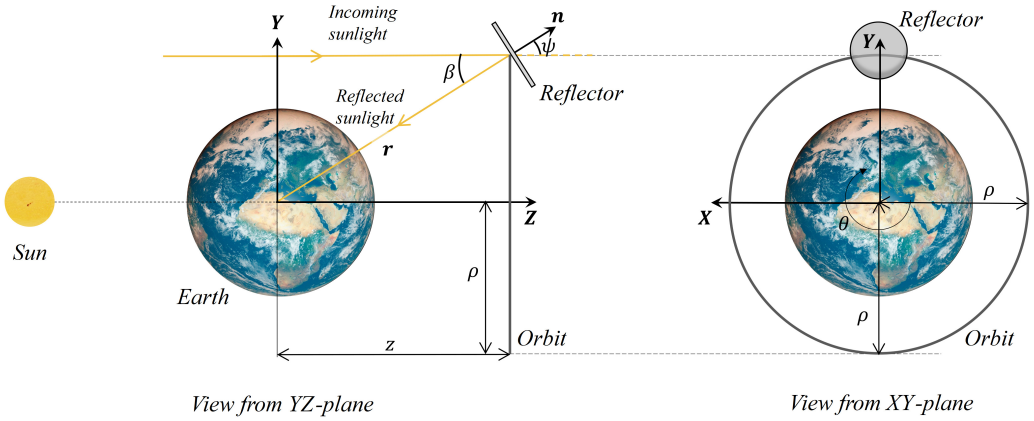

Fig. 1: Schematics of the problem and the rotating reference frame

the SRP acceleration expression, ψ denotes the pitch angle of the reflector, and κ denotes the characteristic acceleration, i.e. $\kappa = 8.43 \times 10^{-3}/\sigma$ mm/s^2 at 1 Astronomical Unit, with σ being the areal density of the reflector in the units of g/m^2. In the rotating reference frame, the first two terms in Eq. 1 would be equal to zero. If, then, the equations of motion Eq. 1 are described in the Earth-centered cylindrical coordinates (ρ, θ, z), such that ρ is the orbit radius, z is the displacement along the z axis, and θ is the azimuth angle, they would take the following form:

$$\ddot{\rho} - \rho\dot{\theta} = -\frac{\mu}{r^3}\rho\left(1 - \frac{3}{2}J_2\left(\frac{R}{r}\right)^2\left(5\left(\frac{\rho}{r}\right)^2 - 2\right)\sin^2\theta - 1\right) + \kappa\cos^2\psi\sin\psi \tag{3a}$$

$$\rho\ddot{\theta} + 2\dot{\rho}\dot{\theta} = -\frac{\mu}{r^3}\rho\frac{3}{2}J_2\left(\frac{R}{r}\right)^2\sin 2\theta \tag{3b}$$

$$\ddot{z} = -\frac{\mu}{r^3}z\left(1 - \frac{3}{2}J_2\left(\frac{R}{r}\right)^2\left(5\left(\frac{\rho}{r}\right)^2\sin^2\theta - 1\right) - 1\right) + \kappa\cos^3\psi \tag{3c}$$

as discussed in [20]. In order to find the equilibrium condition that enables displaced non-Keplerian orbits, θ may be used as the independent parameter and an averaging may be carried out. The substitution $\dot{\mathbf{r}} = \omega(\mathrm{d}\mathbf{r}/\mathrm{d}\theta)$ with $\omega = \dot{\theta}$, and $\ddot{\mathbf{r}} = \omega(\mathrm{d}\omega/\mathrm{d}\theta)(\mathrm{d}\mathbf{r}/\mathrm{d}\theta) + \omega^2(\mathrm{d}^2\mathbf{r}/\mathrm{d}\theta^2)$ may be made into Eq. 1 and the averaging may be performed over a full orbit by using θ, which are omitted here for brevity but can be found fully in Ref. [20]. One can then find the expressions for required pitch angle and the SRP acceleration as in [20]:

$$\tan\psi = \left(\frac{\rho}{z}\right)\frac{1 - \left(\frac{\omega}{\tilde{\omega}}\right)^2}{1 - \frac{3}{2}\frac{\mu}{r^3}J_2\left(\frac{R}{\tilde{\omega}r}\right)^2} \tag{4a}$$

$$\kappa = \tilde{\omega}^2\left(1 - \frac{3}{2}\frac{\mu}{r^3}J_2\left(\frac{R}{\tilde{\omega}r}\right)^2\right)(1 + \tan^2\psi)^{3/2}z \tag{4b}$$

where $\tilde{\omega}$ is angular velocity of the Keplerian orbit with the same radius, ρ and can be expressed with the Earth's oblateness effect included, as:

$$\tilde{\omega} = \sqrt{\frac{\mu}{r^3}\left(1 - \frac{3}{4}J_2\left(\frac{R}{r}\right)^2\left(5\left(\frac{\rho}{r}\right)^2 - 4\right)\right)} \tag{5}$$

As the reflector is intended to direct incoming sunlight from the Sun to the Earth, the pitch angle ψ can also be rewritten as $\psi = \beta/2$, such that [19, 20]:

$$\tan\psi = \tan\left(\frac{1}{2}\tan^{-1}\left(\frac{\rho}{z}\right)\right) \tag{6}$$

Finally, the angular velocity of a displaced NKO can be found for a reflector whose orientation is defined apriori by the fixed pitch angle, ψ:

$$\omega = \tilde{\omega}\sqrt{1 - \left(\frac{z}{\rho}\right)\left(1 - \frac{3}{2}\frac{\mu}{r^3}J_2\left(\frac{R}{\tilde{\omega}r}\right)^2\right)\tan\psi} \tag{7}$$

Note from Eq. 7 that displaced NKOs are slower, i.e. they have longer orbital periods.

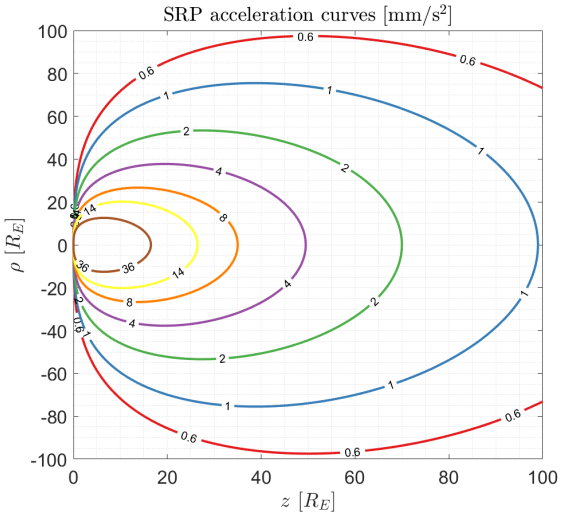

Fig. 2: Curves of solar radiation pressure (SRP) acceleration enabling displaced NKOs

It is now possible to investigate the characteristic acceleration κ values for a given ρ, z pair that enable displaced NKOs, as shown in Fig. 2. Figure 2 shows that both orbits with large radius and small displacement and small radius and large displacement are possible. Large SRP accelerations are required for orbits close to the Earth with large displacements. For orbits with large radius or large displacement, the effect of the Earth's oblateness will decrease with radius. With near-term achievable SRP acceleration values such as $\kappa = 1\,\mathrm{mm\,s^{-2}}$, displacement is limited for small radii orbits. Note that ρ must be equal to at least the Earth's radius for displaced NKOs to be possible by definition, even though in Fig. 2 the value $\rho = 0$ is also included to demonstrate the equilibrium points along the z axis. This requirement also means that displaced NKOs around the Earth are eclipse-free, whose implications will be discussed later. Before, however, dynamics and energy delivery properties of displaced NKOs will be investigated for single reflector systems in the next subsection.

3. Single reflectors in displaced orbits

As outlined in the previous section, the equilibrium conditions dictate a characteristic acceleration and a fixed pitch angle for a selected set of ρ and z. It is in principle possible to find orbits at any radius and displacement even though practical limitations apply when high SRP acceleration is necessary. As the dominant force is the Earth's gravitation, the reflector material needs to be extremely lightweight to achieve large SRP accelerations and displacements. Figure 3 shows the areal density of a reflector necessary for different sets of ρ and z.

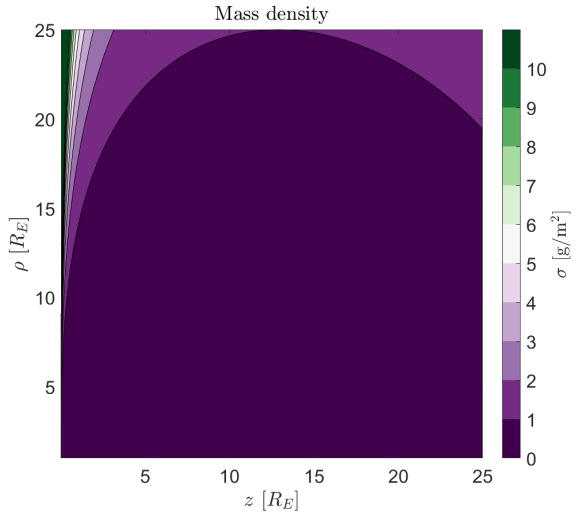

Fig. 3: Areal density required for the displaced orbits

As seen in the figure, less than $1\,\mathrm{g\,m^{-2}}$ is necessary to achieve large displacements. There are regions where the areal density is higher but those regions are also with high orbit radius. With more conservative estimates of $10\,\mathrm{g\,m^{-2}}$, the displacement z is constrained in an extremely small region and at relatively large ρ. To explore the potential of displaced NKOs for space-based solar energy applications, such engineering limitations may be relaxed. Indeed, there are low areal density materials already proposed in the literature that could potentially enable largely displaced orbits [27]. There are already carbon fiber-based materials that could reduce the areal density below $10\,\mathrm{g\,m^{-2}}$ [28]. Primarily motivated by interstellar travel, Drexler et al. proposed materials two orders of magnitude below at $3 \times 10^{-2}\,\mathrm{g\,m^{-2}}$ [29]. More recently, it was proposed that graphene-based materials that could reduce the areal density to values $8.6 \times 10^{-4}\,\mathrm{g\,m^{-2}}$ [30]. At this last value, the SRP acceleration at 1 AU is equal to $10.6\,\mathrm{m\,s^{-2}}$, i.e. larger than the gravitational acceleration on the surface of the Earth. This implies that much smaller radii but highly displaced NKOs could be achieved. However, the stability properties of those need to be investigated further.

3.1 Orbit stability

Salazar et al. [20] investigated the linear stability properties of displaced non-Keplerian polar orbits

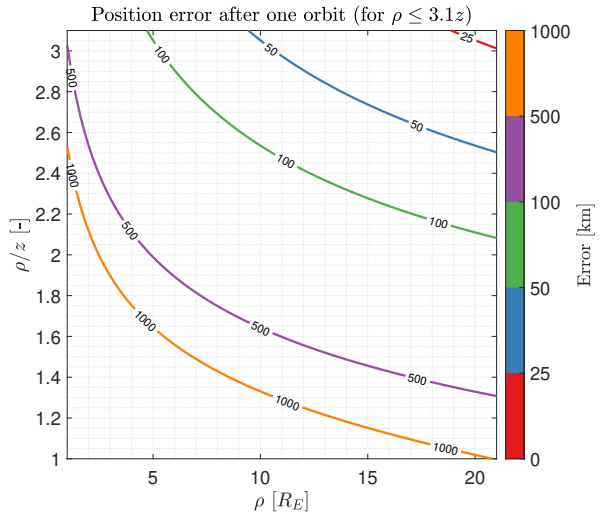

Fig. 4: Position error after one orbit for displaced NKOs with $\rho \leq 3.1z$.

following McInnes [15] and found out that the orbits are linearly stable for the condition

$$\rho > 3.1z \tag{8}$$

The implication of the above stability result is that the reflected image of the solar disk would be very large for stable orbits with large displacements to illuminate solar power farms at night. This is undesired, as the aim is to ensure the maximal use of fixed-size solar power farms. But the unstable orbits drift from their reference orbit very quickly, as shown for orbits with $\rho \leq 3.1z$ in Figure 4.

The minimum ρ value is $1R_E$ in this analysis. No initial perturbation is introduced to the state vector. It is then clear that small ρ/z (i.e, relatively large displacements) would result in more than a 1000 km drift from the start point after one orbit period. Even near the stability boundary, the position error after one orbit is only slightly less than 25 km for the orbit radius of $20R_E$, implying a further drift in subsequent orbits. For the applications considered here, then, unstable families of displaced NKOs will be more effective, therefore their controllability needs to be investigated further.

3.2 Orbit control

Controllability of unstable families of displaced NKOs is assessed for a spherical Earth in Hill's problem by Bookles and McInnes [21]. Here it is considered within the body problem enhanced by the Earth's oblateness term J_2 as the displaced NKOs considered here are closer to the Earth. First, the linearised system is considered as below:

$$\begin{aligned} &\dot{\mathbf{x}} = A\mathbf{x} + B\mathbf{u} \\ &\mathbf{y} = C\mathbf{x} \end{aligned} \quad A = \begin{bmatrix} 0 & 0 & 1 & 0 \\ 0 & 0 & 0 & 1 \\ L_{11} & L_{12} & 0 & 0 \\ L_{21} & L_{22} & 0 & 0 \end{bmatrix}$$
$$B = \begin{bmatrix} 0 \\ 0 \\ \frac{\partial a_\rho}{\partial \kappa} \\ \frac{\partial a_z}{\partial \kappa} \end{bmatrix} \quad C = \begin{bmatrix} 1 & 0 & 0 & 0 \\ 0 & 1 & 0 & 0 \\ 0 & 0 & 1 & 0 \\ 0 & 0 & 0 & 1 \end{bmatrix} \tag{9}$$

where x is the state-space vector, u is the control input, y is the output. The azimuthal symmetry implies that all derivatives with respect to θ vanish [15], such that the 6×6 system reduces to 4×4. In Eq. 9 then, A denotes the constant coefficient matrix of the system, formed from the partial derivatives of the 2×2 Jacobian matrix, as also presented in [20]:

$$\begin{aligned} L_{11} &= 3 + \frac{\mu}{r^3}\left(\frac{1}{\omega^2}\right)\left(1 - \left(\frac{\rho}{r}\right)^2\right) \\ &- \frac{3}{4}\frac{\mu}{r^3}J_2\left(\frac{1}{\omega^2}\right)\left(\frac{R_E}{r}\right)^2\left(\left(1 - 5\left(\frac{\rho}{r}\right)^2\right)\left(5\left(\frac{\rho}{r}\right)^2 - 4\right)\right. \\ &\left. + 10\left(\frac{\rho z}{r^2}\right)^2\right) \\ L_{12} &= -3\frac{\mu}{r^3}\left(\frac{1}{\omega^2}\right)\left(\frac{\rho z}{r^2}\right) \\ &+ \frac{15}{4}\frac{\mu}{r^3}J_2\left(\frac{1}{\omega^2}\right)\left(\frac{R_E}{r}\right)^2\left(\frac{\rho z}{r^2}\right)\left(7\left(\frac{\rho}{r}\right)^2 - 4\right) \\ L_{21} &= L_{12} \\ L_{22} &= \frac{\mu}{r^3}\left(\frac{1}{\omega^2}\right)\left(1 - \left(\frac{\rho}{r}\right)^2\right) \\ &- \frac{3}{4}\frac{\mu}{r^3}J_2\left(\frac{1}{\omega^2}\right)\left(\frac{R_E}{r}\right)^2\left(\left(1 - 3\left(\frac{z}{r}\right)^2\right)\left(5\left(\frac{\rho}{r}\right)^2 - 2\right)\right. \\ &\left. + 4\left(\frac{z}{r}\right)^2\left(1 - 5\left(\frac{z}{r}\right)^2\right)\right) \end{aligned} \tag{10}$$

B is the coefficient matrix of the inputs formed by the partial derivatives of the control acceleration with respect to the desired control parameter. The control is applied in ρ and z. In this paper, small trims in the reflector area are considered as the control method, which changes the SRP acceleration experienced by the reflector. The methods of control include pitch angle control [15, 21], but as the pitch angle is coupled to the location that the light is reflected on the Earth, it may unsuitable for orbiting solar reflector-type applications. Then, the partials in B can be

found as:

$$\frac{\partial a_\rho}{\partial \kappa} = \cos^2\psi \sin\psi \tag{11a}$$

$$\frac{\partial a_z}{\partial \kappa} = \cos^3\psi \tag{11b}$$

Finally, C denotes the output coefficient matrix, which is a 4×4 identity matrix. Controllability of a linear system expressed in the form of Eq. 9 can be found by evaluating the controllability matrix that can be expressed as [31]:

$$M_c = \begin{bmatrix} B & AB & A^2B & A^3B \end{bmatrix} \tag{12}$$

If M_c is full rank, which is equal to 4 in this case, the linear system is considered controllable, i.e. some initial state $\mathbf{x}_0$ is carried to some final state $\mathbf{x}_f$ with the control input $\mathbf{u}$, as discussed in [21]. It is indeed the case here and the linearised system in Eq. 9 is full rank. Following [15], the change in the SRP acceleration due to the reflector area control can then be expressed as:

$$\begin{aligned} \delta\kappa = G_1(\rho - \rho_0) + G_2(z - z_0) \\ + G_3(\dot{\rho} - \dot{\rho}_0) + G_4(\dot{z} - \dot{z}_0) \end{aligned} \tag{13}$$

where G_j (j = 1-4) denotes control gains, ρ_0 and z_0 are the reference states, whereas ρ and z are the current states. As displaced NKOs considered here are circular orbits, ρ_0 and z_0 will be the targeted orbit radius and displacement, and $\dot{\rho}_0$ and $\dot{z}_0$ will be equal to zero.

It is now possible to design a control system. In this paper, a linear optimal control scheme is considered. Using optimal control theory, the following cost function can be used to determine the control gain:

$$J = \int_t^\infty [\mathbf{x}(\tau)' Q \mathbf{x}(\tau) + \mathbf{u}(\tau)' N \mathbf{u}(\tau)] \mathrm{d}\tau \tag{14}$$

where J is the cost function and τ is time. Q is the diagonal matrix associated with the penalty on the deviation from the reference state and N determines the cost of control. The selection of Q and N determines the control system behaviour while reaching the desired state. The goal is to find the control gains that minimise the cost function, which is found by solving the Riccati equation:

$$-\dot{M} = MA + A'M - MBN^{-1}B'M + Q \tag{15}$$

where M denotes the performance matrix and is related to the cost function such that $J = \mathbf{x}'M\mathbf{x}$. It can be assumed that $-\dot{M} \to 0$ for $t \to \infty$. Such a form of Eq. 3.2 is called the Algebraic Riccati Equation and the optimal gains can be found by solving it such that

$$G = N^{-1}B'M. \tag{16}$$

In this paper, `MATLAB`'s `lqr` function is used to compute the optimal gains. The selection of Q and N matrices are generally found empirically, but the general requirement is to select a diagonal Q matrix based on the desired control accuracy, while N is selected to suppress the values of partial derivatives in A matrix. As there is no specific requirement on the level of control accuracy, Q is selected as a 4×4 identity matrix and N is given values between 1×10^{-10} to 1×10^{-13} depending on the desired control behaviour. Figure 5 shows an example of a controlled and uncontrolled orbit alongside the control effort necessary to maintain the orbit.

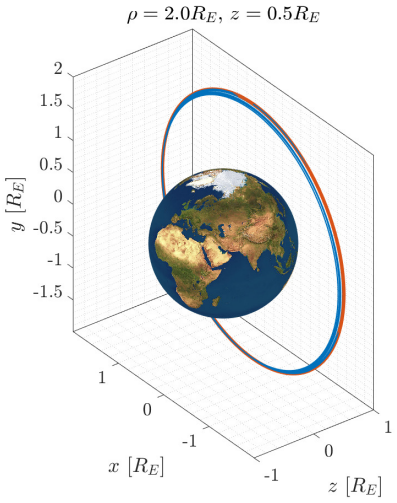

Fig. 5: Unstable orbit controlled by small trims in the reflector area. The blue orbit is the drifting orbit whereas the red orbit is the controlled.

Figure shows a theoretically stable (i.e., $\rho/z > 3.1$) orbit at $\rho = 2R_E$ and $z = 0.5R_E$, but as shown in Fig. 5, the uncontrolled orbit drifts over 10 orbits. But with appropriate control, it can be maintained for the duration of 10 orbit periods simulated here. This requires less than a %0.5 change in the SRP acceleration by the reflector area, as shown in Fig. 6. This may be achievable via tip vanes [15].

In the next section, the properties of the displaced NKOs will be investigated from the perspective of space-based solar energy applications.

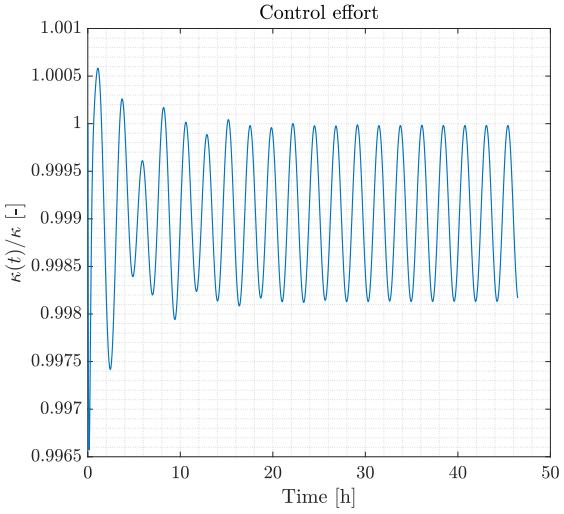

Fig. 6: Control effort normalised with κ

3.3 Solar energy delivery from displaced non-Keplerian orbits

Displaced non-Keplerian orbits possess several unique advantages that may make them suitable for space-based solar energy applications. As noted earlier, displacement in the anti-Sun direction could allow for the delivery of solar energy only at nighttime. This is different than, for example, Keplerian polar orbits, whose right ascension of the ascending node may be tilted towards the nighttime, but this will mean that the other half of the orbit will be tilted towards the dayside of the Earth. Moreover, Keplerian polar orbits would also be limited in such a tilt due to the Earth's eclipse, which displaced NKOs do not experience by their definition. Furthermore, displacement towards nightside also opens up opportunities to deliver solar energy to higher latitude regions, which may be suitable for both solar energy, illumination and other climate-related applications [8, 5, 20].

In order to calculate the quantity of energy delivered, now consider the power that can be delivered to the surface of the Earth as:

$$P_{SPF} = \chi(t) I_0 \frac{A_M}{A_{im}(t)} A_{SPF} \cos\frac{\psi}{2} \tag{17}$$

where I_0 is the solar constant, assumed to be decreasing with an inverse-square law with the distance from the Sun and equal to 1.37 GWkm^{-2} at 1 Astronomical Unit (AU), the mean distance between the Earth and the Sun. A_M, A_{SPF}, A_{im} are the areas of the reflector, solar power farm and solar image reflected on the ground. The area of the solar image is a function of the slant range from the ground target and the angle subtended by the Sun, α (≈0.0093 rad), whose calculation is provided in detail in Ref. [8]. Finally, the time-dependent atmospheric transmission efficiency, $\chi(t)$ is provided with the following empirical relationship [32]:

$$\chi(t) = 0.1283 + 0.7559 e^{-0.3878\sec(\pi/2-\epsilon(t))} \tag{18}$$

where ϵ denotes elevation from the ground target. The energy delivered to the surface can be calculated by integrating Eq. 17 over the desired duration, such that:

$$E = \int_0^t P_{SPF} \mathrm{d}\tau \tag{19}$$

where t is time. As a straightforward example, first, the energy delivered to the surface of the Earth for one orbit period will be considered. Again, such a system may be considered for a mixture of solar energy, illumination and climate-intervention type applications [8, 5, 19, 20]. This calculation will consider a 1-km diameter reflector and no specific ground target, such that the reflector in the displaced orbit will keep its fixed pitch angle dictated by the equilibrium conditions in Eq. 4a and perform no further attitude maneuvers to track the ground target. In such a situation, the solar image reflected on the ground will always be circular, and Eq. 17 will simplify such that the energy delivered can be calculated as

$$E = \bar{\chi} I_0 A_M \cos\left(\frac{\psi}{2}\right) T \tag{20}$$

where $\bar{\chi}$ is fixed atmospheric transmission efficiency at the zenith point, and equal to 0.641, and T is the orbit period. According to this, the energy delivered over one orbit period can be calculated, which is presented for a range of ρ and z in Fig. 7.

Figure 7 shows that, despite the increasing distance from the Earth, the energy delivered increases. The explanation of this result lies in the pitch angle requirements and orbit period of displaced NKOs. ψ decreases for increasing z for a given ρ. This results in the $\cos(\psi/2)$ term taking a higher value. For a Keplerian orbit at the same radius r, the orbit can only be tilted towards the night side until the eclipse limits, and the pitch angle would only be decreased as much. Even then, this would only be beneficial for the half of a Keplerian polar orbit, while the other half will be on the dayside of the Earth, delivering a lower quantity of energy, due to the increased angle between incoming and outgoing sunlight. Moreover, as also noted earlier, displaced NKOs have lower angular velocity

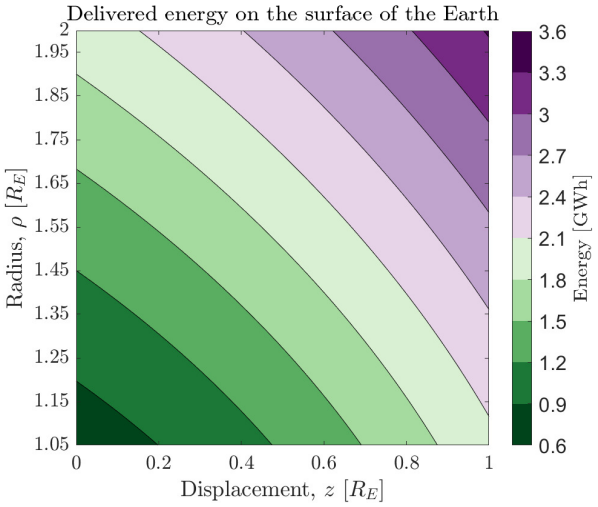

Fig. 7: Solar energy delivery to the surface of the Earth in one orbit period

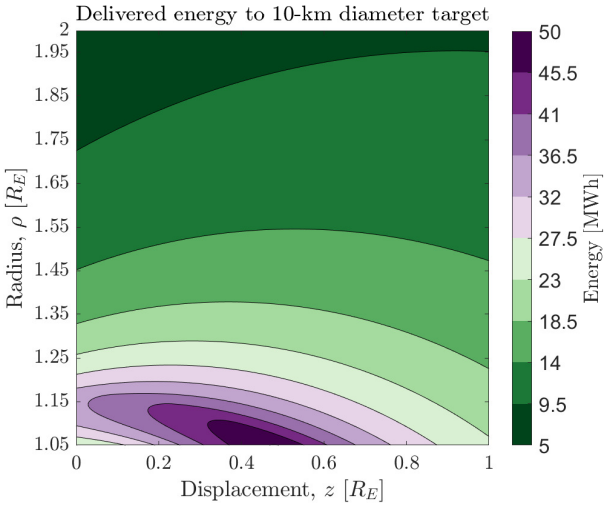

Fig. 8: Solar energy delivery to a 10 km diameter stationary ground target

than their Keplerian polar orbit counterparts at the same r, hence they have longer orbit periods. The combination of the increase in orbit period and the decrease in pitch angle translates as higher energy delivery per orbit for the displaced NKOs, especially as the displacement increases. For an example case of $\rho = 1.15R_E$ (approximately an altitude of 957 km) and $z = 0.1R_E$, the quantity of energy delivered to the surface of the Earth is approximately 0.92 GWh per orbit. The period of this orbit is 1.18 h, then the energy delivered per day can be found as approximately 12.13 GWh.

The results of the analysis can also be considered for the case of a solar power farm as the ground target. This would be an example of a space-based solar energy application via orbiting solar reflectors. The target will be assumed as a stationary point on the Earth, i.e., the Earth's rotation will be assumed negligible. While this is clearly not true in reality, the calculations will provide an upper limit on the deliverable energy to the ground. A circular solar power farm of 10 km diameter is assumed with flat solar panels, but the full time-varying geometry of the pass and atmospheric efficiency (as provided in Eq. 18) will be included. The calculation follows the methodology presented in Çelik and McInnes [8] and adapted for the displaced orbit cases here and the results are presented in Fig. 8.

An optimum point of maximised energy delivery is evident from Fig. 8, where the quantity of the energy delivered is equal to approximately 50 MWh from the displaced NKOs at ρ=$1.05R_E$ and z=$0.48R_E$ with the distance of $r = 1.1545R_E$ (approximately 986 km for the surface of the Earth). Such displacement with small ρ would require nearly $5\,\mathrm{m\,s^{-2}}$ of SRP acceleration, which is challenging to achieve with currently available technology. If a smaller z and a higher ρ are selected, the SRP acceleration required can be decreased, which will also mean a decrease in the quantity of energy delivered, but may be more feasible. For example, a 1-km reflector at a displaced NKO with $[\rho,\ z] = [1.2518R_E,\ 0.0001R_E]$ (approximately at 1606.6 km altitude with 0.637 km displacement) would deliver 23.5 MWh energy while the energy delivered from the Keplerian polar orbit of the same altitude would be equal to approximately 22 MWh. The SRP acceleration required for such a modest displacement will be $1.41\,\mathrm{mm\,s^{-2}}$. This would then require a reflector with an areal density of approximately $6.5\,\mathrm{g\,m^{-2}}$, which is in principle achievable with current technology, as noted earlier. Moreover, this result suggests not only the feasibility of such a space-based solar energy application, but also suggests that it may even be preferable given that the quantity of the energy delivered is higher for the displaced orbit, compared to a Keplerian polar orbit of the same altitude. It is worth noting that attitude maneuovres will be necessary to track the solar power farm. In the case of a non-stationary ground target, attitude tracking will likely include pitch angle maneuovres as well. The changes in the pitch angle will alter the equilibrium condition set for the displaced orbits, which could be counteracted by using flap-type structures on the reflectors to cancel the

unbalanced SRP force.

As a further note, the utility of the reflectors in displaced NKOs can be increased by using repeating ground track (RGT) orbits. Those are orbits that complete an integer number of revolutions in a given period of time, such that they come back to the same point at the end [33]. The RGT condition is a function of the orbit period, hence the distance from the centre of the Earth, r. In the case of displaced NKOs, the same r can be achieved for different combinations of ρ and z, therefore multiple choices are available. For more modest displacements that could be achieved by near-term technologies, the RGT orbit distance from the centre of the Earth will be approximately the same as the Keplerian orbit radius, therefore further analysis is not provided here. A more in-depth analysis of the RGT orbit selection in the J_2-enhanced orbits is provided in Ref. [10].

Another way to increase the quantity of energy delivered to a solar power farm is to utilise a compound reflector system, which will be discussed next.

4. A novel application: Compound reflector system

The compound reflector concept in this paper refers to a system of two reflectors, of which one is a Sun-facing parabolic primary reflector, displaced in the anti-Sun direction by exploiting the SRP force. This parabolic reflector focuses the intercepted light from the Sun to the secondary flat reflector, which is displaced in the Sun direction by the SRP force generated by the focused light from the primary reflector. The motion of the two reflectors will therefore need to be synchronised. An illustration of this concept is provided in Fig. 9.

The advantage of this concept is that the separation of focusing and directing functions, which is optically challenging for a standalone parabolic reflector that is both the Sun- and the Earth-facing and performing attitude maneouvers at the same time. By separating these functions, losses in power density on the ground due to the reflected solar image by the flat reflector may be compensated and much higher quantities of energy delivery to the ground may be achieved. For realistic SRP accelerations, the displacement of both sides of the terminator line is expected to be small, such that energy will primarily be delivered around the dawn/dusk hours by the secondary reflector. In order to achieve this, first, the orbital conditions of this compound system will be discussed more in detail in the next subsection.

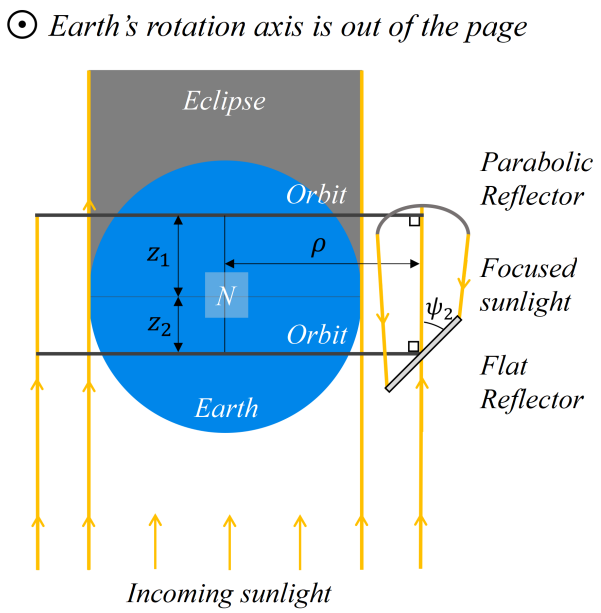

Fig. 9: Illustration of the compound reflector concept (image not to scale)

4.1 The conditions for the compound system orbits

The orbit of the proposed compound system must satisfy multiple requirements. The primary reflector is considered to be Sun-facing and displaced along the Earth-Sun line in the anti-Sun direction at an orbit radius ρ and displacement z_1. The secondary reflector will face the primary reflector and be placed along the same line, such that it will have the same ρ. The reflectors will also be in synchronised motion, such that the angular velocity of the reflector orbits will be equal. The displacement of the secondary reflector in the Sun direction, z_2, will be the parameter, controlled by the SRP acceleration and the fixed pitch angle, ψ_2. The orbit design requirements can then summarised as follows:

- The primary reflector pitch angle, ψ_1 shall be equal to 0
- The displaced orbit radius, ρ, of both reflectors shall be the same
- The angular velocity of both orbits shall be the same

Note that for the remainder of this section subscripts 1 and 2 will be used to denote parameters related to the primary and the secondary reflectors, respectively. To select an orbit for the primary reflector, now consider Eq. 4a, and substitute $\psi_1 = 0$, such

that $\tan\psi_1 = 0$. The only condition that satisfies this in Eq. 4a is

$$\omega = \tilde{\omega}_1 \tag{21}$$

where ω is now considered to be the system angular velocity for the synchronised motion. The SRP acceleration for the primary reflector can also be found from Eq. 4a as

$$\kappa_1 = \tilde{\omega}_1^2 \left(1 - \frac{3}{2}\frac{\mu}{r_1^3} J_2 \Big(\frac{R_E}{\tilde{\omega}_1 r_1}\Big)^2\right) z_1 \tag{22}$$

The SRP acceleration in the case of the primary reflector is only a function of z_1 for a given ρ. If the achievable SRP acceleration is known or desired to be restricted, the maximum z_1 can be found by rearranging Eq. 22 and solve for z_1. In the case of a spherical Earth, the J_2-related term will disappear and the SRP acceleration on the primary reflector will be equal to $\kappa_1 = \tilde{\omega}_1^2 z_1$.

The secondary reflector displacement z_2 can be found by considering the synchronised motion requirement. As shown above, if the system angular velocity $\omega = \tilde{\omega}_1$, then the orbit angular velocity of the secondary reflector must satisfy the following from Eq. 7:

$$\tilde{\omega}_1 = \tilde{\omega}_2 \left[1 - \Big(\frac{z_2}{\rho}\Big)\Big(1 - \frac{3}{2}\frac{\mu}{r_2^3} J_2 \Big(\frac{R}{\tilde{\omega}_2 r_2}\Big)^2\Big) \tan\psi_2\right]^{1/2} \tag{23}$$

Equation 6 may also be substituted in Eq. 23, which yields

$$\tilde{\omega}_1 = \tilde{\omega}_2 \Big[1 - \Big(\frac{z_2}{\rho}\Big)\Big(1 - \frac{3}{2}\frac{\mu}{r_2^3} J_2 \Big(\frac{R_E}{\tilde{\omega}_2 r_2}\Big)^2\Big) \tan\Big(\frac{1}{2}\tan^{-1}\Big(\frac{\rho}{z_2}\Big)\Big)\Big]^{1/2} \tag{24}$$

Rearranging Equation 24 would finally yield

$$\frac{r_1^3(1-K_{12})}{r_2^3(1-K_{11})}\Big[1 - \Big(\frac{z_2}{\rho}\Big)\Big(1 - K_{22}\Big) \tan\Big(\frac{1}{2}\tan^{-1}\Big(\frac{\rho}{z_2}\Big)\Big)\Big] = 1 \tag{25}$$

where K_{1j} and K_{2j} ($j = 1, 2$ for the primary and secondary reflectors, respectively) are the J_2-related terms such that

$$K_{1j} = \frac{3}{4} J_2 \Big(\frac{R_E}{r_j}\Big)^2 \Big(5\Big(\frac{\rho}{r_j}\Big)^2 - 4\Big) \tag{26a}$$

$$K_{2j} = \frac{3}{2}\frac{\mu}{r_j^3} J_2 \Big(\frac{R_E}{\tilde{\omega}_j r_j}\Big)^2 \tag{26b}$$

Note that for a spherical Earth, all K_{1j} and K_{2j} terms would vanish from Eq. 25. For a given set of ρ-z_1 then, the secondary reflector displacement, z_2 can be found by solving Eq. 25. An immediate result that can be deduced is that if $\psi_2 = 0$, the reflectors would be displaced by the same amount, such that $z_1 = |z_2|$. Equation 25 can also be solved numerically for a range of ρ and z_1 values to find other z_2 values and the results are presented in Fig. 10.

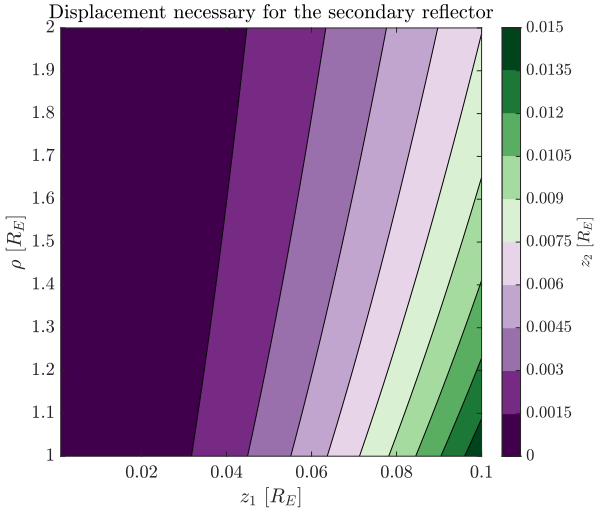

Fig. 10: Displacement of the secondary reflector

In Fig. 10, the x- and y-axes show z_1 and ρ, respectively, whereas the coloured contour shows z_2, where all distances are normalised with respect to the Earth's radius, R_E. For relatively large orbit radii (up to $2R_E$) and displacements up to $0.1R_E$, z_2 is within $0.015R_E$ or approximately 96 km from the terminator line in the Sun direction, i.e. less than 1 deg longitude difference at the equator. Therefore, the secondary reflector will still be in the vicinity of the Earth's terminator line. The displacement increases particularly for smaller ρ and larger z_1. The SRP acceleration will also be higher for such large displacements, which is calculated by substituting z_2 and the resulting ψ_2 in Eq. 4a. The results are shown in Fig. 11.

Note the y-axis in Fig. 11, which is now z_2 and the coloured contour shows the SRP acceleration in $\mathrm{mm\,s^{-2}}$. Three white lines in the figure are provided to denote 1, 10 and $20\,\mathrm{mm\,s^{-2}}$. $1\,\mathrm{mm\,s^{-2}}$ is approximately the SRP acceleration for a $10\,\mathrm{g\,m^{-2}}$ areal density reflector. For the former two values, the displacement is very limited, but greater displacement can be enabled for higher values. Considerable displace-

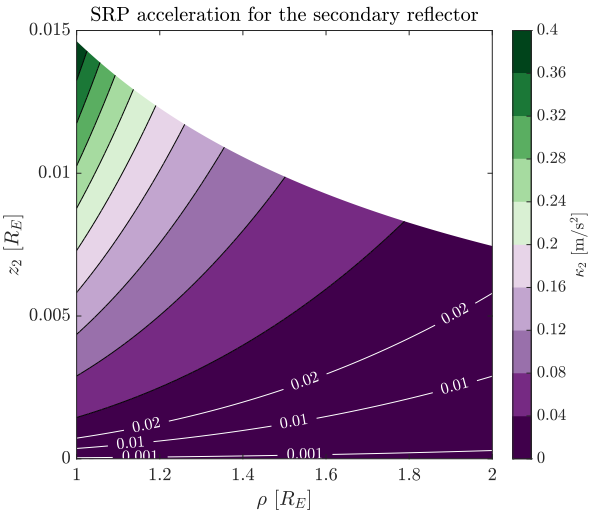

Fig. 11: The SRP acceleration on the secondary reflector

ment may in principle be achieved with $40\,\mathrm{m\,s^{-2}}$ of SRP acceleration, especially for relatively high ρ, up to $1.8R_E$ (or approximately of 5103 km altitude from the Earth's surface), which may be feasible to achieve with a focusing system such as the parabolic primary. The pitch angle results of the secondary reflector, ψ_2, are omitted here for conciseness. However, its value varies around 45 deg, in accordance with the small z_2 around the terminator region. By using these results, example orbits for the compound system are numerically simulated and presented in Fig. 12.

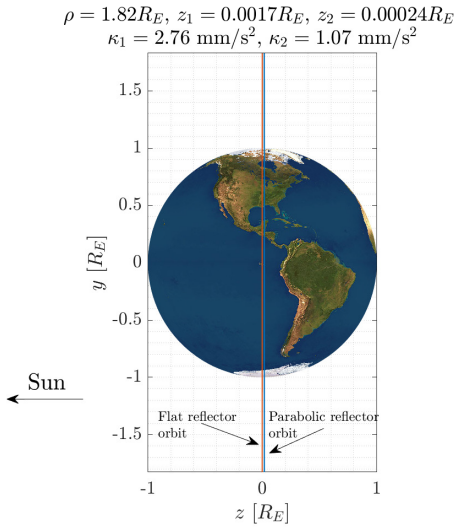

Fig. 12: Example orbits of the parabolic and flat reflectors or the compound system

The orbit radii are $\rho = 1.82R_E$ and the primary displacement is $z_1 = 0.0017R_E$ ($\approx 108.43\,\mathrm{km}$) which results in $z_1 = 0.00024R_E$ ($\approx 1.53\,\mathrm{km}$). The SRP accelerations are $\kappa_1 = 2.76\,\mathrm{mm\,s^{-2}}$ and $\kappa_2 = 1.07\,\mathrm{mm\,s^{-2}}$, respectively. It is worth noting that the SRP from the Sun that is pushing the secondary in the anti-Sun direction is ignored in the simulations, relative to the SRP from the focused sunlight from the primary parabolic collector acting on the smaller secondary reflector. Both orbits are within the stable region (ρ/z >3.1) but as shown in the previous sections, even the unstable family of orbits can be controlled via small trims to the reflector area. In order to realise these compound reflector orbits, the orbital conditions discussed in this section dictate the size of the parabolic primary and secondary. These aspects will be discussed next.

4.2 The sizing of the compound system

The sizing of the compound system consists of determining the shape and areal density of the parabolic primary reflector and the flat secondary reflector. These values are not fixed but are determined by the separation between the reflectors, hence the SRP acceleration. One of the other advantages of such a compound system is that the flat secondary can be relatively small in size, as the capability of focusing through the primary reflector means higher intensity sunlight. To that end, another consideration is that the flat secondary will not be at the focus of the parabolic primary. It is clear that at the focus, the solar power density would in principle be infinite. Instead, it will be assumed that the flat reflector is at some point between the parabolic reflector and its focal point, as shown in Fig. 13.

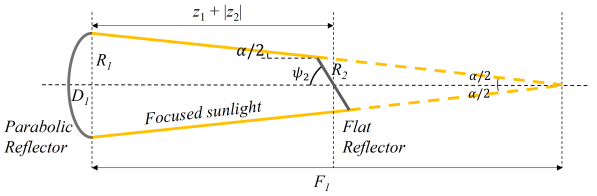

Fig. 13: Sizing of the primary parabolic reflector

The following procedure will be applied in finding the properties of the compound reflectors. First, from the SRP acceleration necessary for the secondary reflector, the artificially generated solar power density by the parabolic primary will be found, such that

$$I_2 = \frac{\kappa_2 c \sigma_2}{2\cos^2\psi_2} \tag{27}$$

where c is the speed of light, equal to $3 \times 10^5\,\mathrm{km\,s^{-1}}$. σ_2 is the areal density of the secondary reflector, here it will be assumed $\sigma_2 = 10\,\mathrm{g\,m^{-2}}$ without any specific material considerations. Note that this value is assumed to demonstrate the procedure. I_2 can easily be found for other values of σ_2 from Eq. 27, as well. It is also worth noting that I_2 should also satisfy the relationship

$$I_2 = I_0 \frac{A_1}{A_2} \tag{28}$$

where A_1 and A_2 are the areas of the primary and secondary reflectors, respectively. The I_2 values are then presented for different ρ and z_1 and the resulting z_2 in Fig. 14.

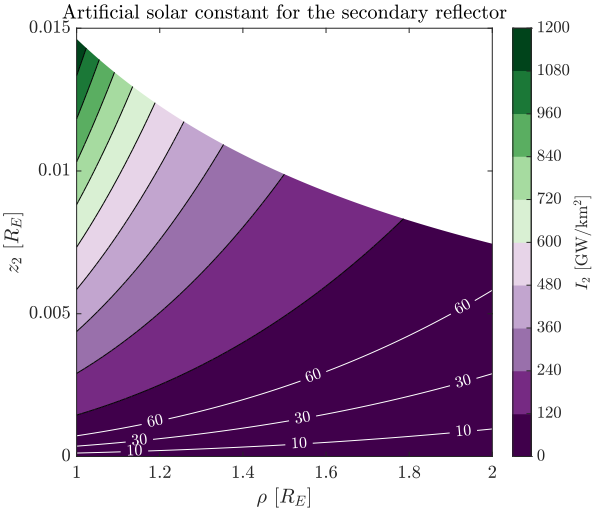

Fig. 14: Generated solar constant on the secondary reflector

As a reference, the solar constant is equal to 1.37 $\mathrm{GWkm^{-2}}$ at 1 AU. It is clear that artificially generated solar constant values are at least a few orders of magnitude higher than I_0. This suggests that very thin, low areal density materials may not be able to withstand such intensities. Higher areal density materials would also mean much higher solar power densities for the same amount of displacement. There are solar sail materials proposed to be able to withstand a heat flux equivalent to 25 times the SRP at 1 AU, i.e, approximately equivalent to the distance between the Sun and Mercury [34]. It would then be possible to find materials to achieve displacements around the terminator region, which is primarily targeted in this paper. On the other hand, I_2 can be decreased by larger reflectors, as per Eq. 28, but this would result in a higher subtense angle by the parabolic reflector, increasing the size of the projected solar image on the ground.

Next, a radius R_2 will be assumed for the secondary reflector. Again, for demonstration purposes, R_2 is fixed to 100 m. The primary area can then be found by substituting I_2 and A_2 in Eq. 28. The calculated A_1 should also satisfy the following relationship from the area of a circular paraboloid:

$$A_1 = \frac{\pi R_1^2}{6D_1^2}\left(\left(R_1^2 + 4D_1^2\right)^{3/2} - R_1^3\right) \tag{29}$$

where R_1 is the rim radius of the circular paraboloid and D_1 is its depth. A parabola also satisfies the following relationship:

$$R_1^2 = 4F_1 D_1 \tag{30}$$

where F_1 is the focal length of the parabola. One can now rearrange Eq. 30 to rewrite D_1 as $D_1 = R_1^2/4F_1$. Substituting this in Eq. 29 and rearranging to find R_1 yield

$$R_1 = \left[F_1\left(\frac{3A_1}{2\pi F_1} + 1\right)^{2/3} - 1\right]^{1/2} \tag{31}$$

From Fig. 13, one can also note the relationship between F_1 and R_1 from the triangle geometry

$$R_1 = \frac{F_1}{\tan(\alpha_2/2)} \tag{32}$$

where α_2 is the angle subtended by the primary reflector at the distance $z_1 + |z_2|$ as

$$\alpha_2 = 2\arctan\frac{R_1 + R_2\sin\psi_2}{z_1 + |z_2|} \tag{33}$$

Substituting Eq. 32 and 33 in Eq. 31 would finally yield

$$R_1 = \left[\frac{R_1\left(z_1 + |z_2|\right)}{R_1 + R_2\sin\psi_2}\left(\frac{3A_1}{2\pi}\frac{R_1\left(z_1 + |z_2|\right)}{R_1 + R_2\sin\psi_2} + 1\right)^{2/3} - 1\right]^{1/2} \tag{34}$$

The rim radius R_1 can then be found by solving Eq. 34 for a given secondary radius R_2. The focal length F_1 and the parabola depth D_1 can also be found by using Eqs. 32 and 30.

This procedure ensures that the focal point of the parabolic reflector is always at a distance greater than the distance between the two reflectors such that the flat reflector is guaranteed to be illuminated. The

procedure also selects the minimum R_1, and the corresponding D_1, is to ensure that A_1 intercepts the amount of sunlight necessary to deliver that onto the flat secondary reflector. Higher R_1 could be selected, then D_1 will also increase accordingly. Figure 15 below shows the rim radius necessary to achieve z_2 for a given $\rho \in [1R_E, 2R_E]$ and $z_1 \in [1 \times 10^{-5}R_E, 0.1R_E]$.

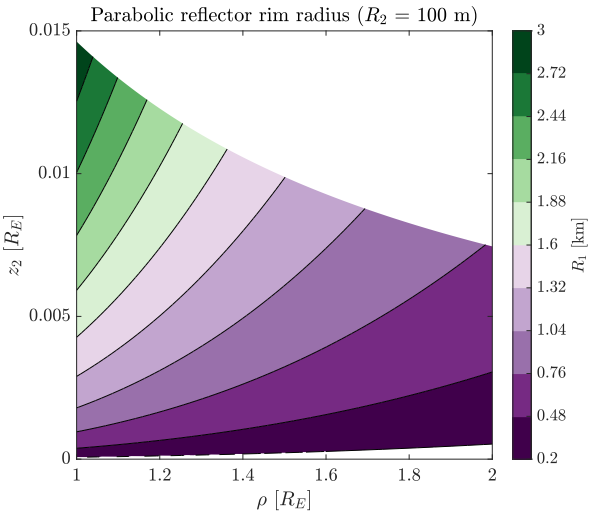

Fig. 15: Rim radius as a function of ρ and z_2 (Colorbar label should be km)

Note in Fig. 15 that there is now an infeasible region for extremely small displacements z_2. Those are the displacements for which the SRP accelerations necessary are below that of the flat reflector can receive from the Sun directly, such that there is no need for the focusing functionality. This means that $I_2 < I_0$. The maximum rim radius is found to be approximately 3 km for relatively large displacements of the secondary reflector, but such displacements require much higher SRP accelerations that may not be achievable for currently available technology. For more achievable SRP accelerations, Fig. 15 shows that the rim radius can be between 0.2 and approximately 0.5 km for small displacements. Full shape properties for the parabolic reflector are presented in Fig. 16.

In accordance with the orbit displacements, F_1 can take values from a few tens of kilometers to slightly more than 700 km. A potentially more interesting result, however, is very small parabola depths. D_1 is within half a meter for parabolic reflectors with R_1 of up to 1.5 km. The maximum value is approximately 3.2 m for nearly a 3-km rim radius parabola.

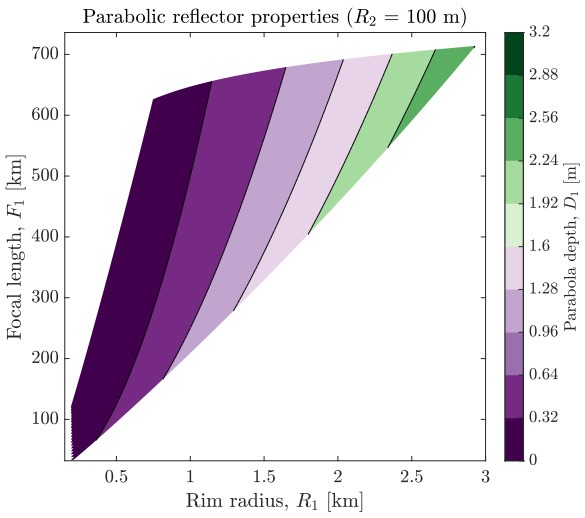

Fig. 16: Shape properties of the primary reflector

These can be considered almost flat reflectors. Small D_1 suggests that the primary reflector may be a relatively simple system, consisting of a hoop of radius R_1, with a slack low areal density membrane attached to the hoop. It has been shown that reflectivity modulators across the reflector surface can generate the desired parabola depths in Fig. 16 by controlling the SRP-induced acceleration across the membrane [35, 36]. These studies demonstrate that the depth-to-radius ratio of up to 0.3 is possible with R_1 values of approximately 100 m [35, 36]. The R_1 values are higher in this study, but a much smaller depth-to-radius ratio suggests that this may be achievable. Such a system may eventually allow solar energy to be focused on the secondary flat reflector, and within the feasibility envelope. Significant solar energy can then be delivered to the surface of the Earth, which will be quantified in the next subsection.

4.3 The energy delivery properties of the compound system

As with the single reflectors in displaced NKOs, the quantity of solar energy delivered will now be discussed as the total quantity delivered to a stationary target on the Earth, and the surface of the Earth, over an orbit period, while the reflector is always assumed to be in the zenith position. The primary differences between the single and the compound reflector systems are that the solar constant I_0 in Eq. 17 will be replaced with I_2, generated by the parabolic primary reflector. Similarly, the subtense angle, α, is now calculated as the angle subtended by the parabolic

reflector, denoted as α_2, which is used to calculate the area of the solar image. The flat reflector's pitch angle ψ_2 is also calculated according to the necessary displacement. The maximum displacement will be the same as the values considered throughout this paper as presented in Fig. 10. Such small displacements mean that the reflectors will be within 1 deg longitude from the terminator region in the Sun direction, as noted earlier. Finally, the flat secondary reflector will be assumed circular with 100 m radius. Note once again that the calculation follows the procedure outlined in Çelik and McInnes, adapted for the displaced NKO case [8].

The quantity of energy delivered is first presented for the case of the flat reflector at a fixed pitch angle and pointing to the centre of the Earth, such that it projects a circular area of the solar image coming from the parabolic reflector at the zenith position, as shown in Fig. 17.

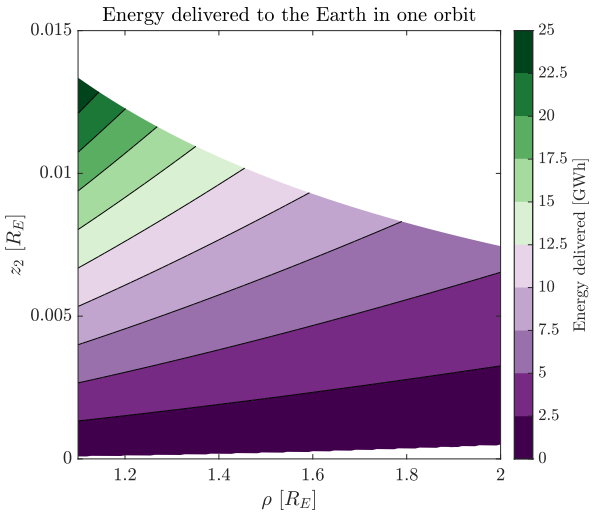

Fig. 17: The quantity of solar energy delivered to the surface of the Earth over one orbit

Figure 17 presents the results for one orbit period. In general, up to 25 GWh of solar energy can be delivered to the surface of the Earth. For small displacements, this value is less than 2.5 GWh, but still similar to values that can only be achieved by a single reflector at very large displacements in the anti-Sun direction. The prime contributor to this result is I_2, which is at least 10 times higher than I_0 for feasible cases. For small focal lengths as a result of small displacements, α_2 is generally greater than the angle subtended by the Sun at 1 AU, i.e., 0.0093 rad. This would result in a larger area of the solar image, but that appears to be compensated by I_2 primarily, as well as ψ_2 and increased orbit period. As the displacements increase, α_2 decreases below that of 0.0093 rad, which then makes the circular area of the solar image smaller than that of those with single reflectors at the same radius from the centre of the Earth, increasing the quantity of energy delivered further.

A similar analysis can be performed for the quantity of energy delivered to a 10-km stationary ground target for a space-based solar energy application, which is presented in Fig. 18.

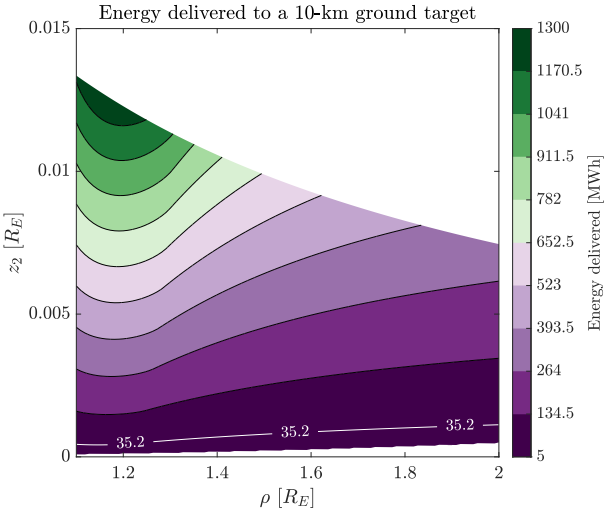

Fig. 18: The quantity of solar energy delivered to a stationary 10-km ground target.

The quantity of energy delivered can be as small as 5 MWh and up to 1.3 GWh depending on the secondary reflector displacement. Similar to the results presented in Fig. 17, the increased I_2 and orbital period, together with decreasing ψ_2 and α_2 (at least after a certain displacement) result in a considerably enhanced quantity of solar energy delivered, as compared to single reflectors in displaced NKOs and Keplerian polar orbits discussed in Ref. [8]. The GWh-level quantity of energy is directly comparable to the levels of solar power satellites, such that the compound system may in principle provide the baseload levels power from LEO, provided that the solar power intensity on the flat reflector (as shown in Fig. 14) can be overcome and the parabolic reflector can be displaced, by the choice of appropriate reflector materials for each of them. Such significant energy delivery would likely mean high illumination on the ground, however. Figure 18 shows a reference line representing the maximum quantity of en-

ergy delivered (approximately 35.2 MWh) from Keplerian polar orbits at approximately 930 km altitude [8]. A similar or higher quantity of energy can be delivered from higher orbit altitudes (i.e., $\rho > 1.15R_E$) with only modest displacements. Moreover, within the displacements of $z_2 = 0.0025R_E$ or 16 km, the quantity of energy delivered could be as high as 134.5 MWh, which is nearly a 4-fold increase compared to the maximum quantity found in the Keplerian polar orbit case [8]. The SRP acceleration necessary for such displacements is within $10\,\mathrm{mm\,s^{-2}}$, from Fig. 11. If this can be achieved, a significantly higher quantity of additional solar energy may be available in the dawn/dusk times of the day for solar energy generation.

4.4 A discussion on the design of a compound system

The design of a compound system is a multifaceted problem, as demonstrated in the previous subsections. Unlike typical SPTs where all components of the spacecraft are connected by a boom [22], the orbit displacement necessary on both sides of the terminator line imposes different design requirements for the parabolic primary reflector and the flat secondary.

On the one hand, the displacement towards the nightside is very limited with the reflector materials currently available. For example, approximately 0.6 km displacement at an altitude of 1600 km will require the SRP acceleration of $1.41\,\mathrm{mm\,s^{-2}}$ and approximately $6.5\,\mathrm{g\,m^{-2}}$ reflector material, as discussed earlier. To enable the primary's displacement in Fig. 12, the necessary areal density is approximately $3.3\,\mathrm{g\,m^{-2}}$. These are some of the materials that may in principle be manufactured by the currently available or near-term technologies [28]. However, as shown in Fig. 18, the quantity of energy delivered could be enhanced significantly if slightly higher displacements are achieved. This would require materials of the areal densities below $\mathrm{g\,m^{-2}}$ for relatively modest increases in displacement. Such possibilities are discussed in the literature extensively, as outlined in Sec. 3, and reaching even lower values is not beyond the realm of possibilities with developments in nanomaterials [37]. It is important to note that the improvements in low areal density materials go hand in hand with the quantity of solar energy that could be delivered, and higher displacements for the parabolic collector could, in principle, enable orders of magnitude increase in the quantity of solar energy can be achieved with much lower mass to be in the LEO altitudes.

On the other hand, the secondary reflector needs to satisfy a different set of requirements. Low areal density materials would still be desirable, albeit with less demand, such that it can be achievable with near-term technologies. But the main design driver of the secondary is the thermal loads experienced. The solar power density can be easily a few orders of magnitudes higher than that of the solar constant. The materials then need to have high thermal emissivity, highly reflective but also relatively low areal density. Typical materials currently used in solar sails (e.g., Mylar, CP1 and Kapton) have all relatively low melting temperatures compared to the expected temperatures on the order of 900 K or higher [37]. The problem at hand is then similar to solar sails that fly by the Sun at very close distances to enable faster interplanetary or interstellar missions [37]. For really high solar power densities at the secondary ($I_2 \sim$100 $\mathrm{GWkm^{-2}}$ or 100 $\mathrm{kWm^{-2}}$), the materials that can be used are limited, some alternatives such as TiN or W are proposed [37]. Even though these are relatively high-density materials, the mass that will be launched into the LEO altitudes will still be much lower than, for example, a small Solar Power Satellite, to deliver solar energy potentially as high as 400 MWh (as shown in Fig. 18).

It is clear that high quantities of solar energy delivered to the ground will also mean high illumination ground. In LEO altitudes, high illumination is only experienced near the zenith point of an orbital pass [8, 10]. Moreover, the quantity of energy delivered will be decreased due to non-ideal reflectors, especially due to double reflection from the primary and secondary reflectors, even though no drastic decrease in illumination is expected. Furthermore, the increase in the quantity of energy achieved than to the compound system is partially thanks to the decreased subtense angle as compared to that of the Sun at the Earth, so that the area of stray light will actually be decreased as compared to single reflectors in Keplerian or displaced orbits. Nevertheless, a further decrease in the size of the solar image may be achieved by a collimating dual reflector system [22], which would increase the solar power density on the ground but decrease the stray light area.

5. Conclusions

The concept of orbiting solar reflectors could offer a new space-based global energy service to enhance the output of terrestrial solar power farms. They can be used to reflect incoming sunlight onto solar power farms to illuminate them locally. The solar radiation pressure-induced force experienced by the

reflectors in polar orbits can displace the orbits in the anti-Sun direction (i.e., towards the nightside of the Earth) when the reflectors are at a fixed pitch attitude in a rotating reference frame, resulting in a family of orbits called displaced non-Keplerian orbits (also known as terminator orbits in different sources). These orbits are eclipse-free by definition and are in principle be useful for nighttime and high latitude solar energy delivery.

First, the results from previous studies on the dynamics and stability properties of displaced NKOs in two-body dynamics enhanced with the Earth oblateness and the SRP force are reviewed. Most orbits that may be useful for solar energy applications are unstable. They are shown to be controllable and an optimal linear control by reflector area control is proposed. The quantity of energy delivered from a range of displaced NKOs by a 1-km reflector is investigated. When a 10-km stationary solar power farm on the Earth is considered, an increase in the quantity of energy delivered can be achieved compared to the Keplerian polar orbit of the same radius, only with a modest displacement. This is thanks to decreased pitch angle and increased orbital period.

As a novel application, a compound reflector system is proposed. Such a system consists of a parabolic primary reflector displaced in the anti-Sun direction, focusing the intercepted sunlight onto a flat secondary reflector, displacing it in the Sun direction. The compound system offers the advantage of using a parabolic reflector to increase the solar power density but also avoids the optical challenges of standalone parabolic systems by separating focusing and directing functionalities. The equations for the synchronised motion of the reflectors are presented and a procedure is offered to size the combined system. The quantity of energy delivered can in principle be increased by orders of magnitudes by a compound system, but even with extremely modest displacements, a compound system can offer a similar or higher quantity of energy delivered than a Keplerian polar orbit at multiple different altitudes. This is enabled by the combinations of increased solar power density, the decreased subtense angle and secondary pitch angle. This would be achievable by a pair of almost flat, parabolic primary and small flat reflectors.

Displaced NKOs for both single and compound reflectors may potentially enhance the quantity of solar energy delivered to the Earth. The large displacements necessary to enhance the solar energy by orders of magnitudes will require low areal density materials for the primary reflector and high thermal emissivity materials for the secondary reflectors, which are not immediately available, but in pirnciple possible with near-term technologies. Nevertheless, currently available technologies could allow the reflectors to be displaced around the Earth's terminator line, thereby enhancing the utility of solar energy around dawn/dusk times when the terrestrial solar energy contribution is extremely low but the demand may be high.

Acknowledgments

This project has received funding from the European Research Council (ERC) under the European Union's Horizon 2020 research and innovation programme (grant agreement No. 883730). CRM is also supported by the Royal Academy of Engineering under the Chair in Emerging Technologies scheme.

References

[1] Hermann Oberth. Methods of space travel. *Munich, Oldenburg*, page 494, 1929.

[2] Onur Çelik, Andrea Viale, Temitayo Oderinwale, Litesh Sulbhewar, and Colin R. McInnes. Enhancing terrestrial solar power using orbiting solar reflectors. *Acta Astronautica*, 195:276–286, 2022.

[3] Kenneth W Billman, William P Gilbreath, and Stuart W Bowen. Introductory assessment of orbiting reflections for terrestrial power generation. Technical Report NASA-TM-73230, NASA, 1977.

[4] Krafft A. Ehricke. Space light: space industrial enhancement of the solar option. *Acta Astronautica*, 6(12):1515–1633, 1979.

[5] John E Canady and John L Allen. Illumination from space with orbiting solar-reflector spacecraft. Technical Report NASA-TP-2065, NASA, 1982.

[6] Lewis M Fraas, Geoffrey A Landis, and Arthur Palisoc. Mirror satellites in polar orbit beaming sunlight to terrestrial solar fields at dawn and dusk. In *2013 IEEE 39th Photovoltaic Specialists Conference (PVSC)*, pages 2764–2769, Tampa, FL, 2013. IEEE.

[7] Federica Bonetti and C McInnes. Space-enhanced terrestrial solar power for equatorial regions. *Journal of Spacecraft and Rockets*, 56(1):33–43, 2019.

[8] Onur Çelik and Colin R McInnes. An analytical model for solar energy reflected from space with selected applications. *Advances in Space Research*, 69(1):647–663, 2022.

[9] Temitayo Oderinwale and Colin R McInnes. Enhancing solar energy generation and usage: Orbiting solar reflectors as alternative to energy storage. *Applied Energy*, 317:119154, 2022.

[10] Andrea Viale, Onur Çelik, Temitayo Oderinwale, Litesh Sulbhewar, and Colin R. McInnes. A reference architecture for orbiting solar reflectors to enhance terrestrial solar power plant output. *Advances in Space Research (submitted)*.

[11] Andrea Viale, Onur Çelik, Temitayo Oderinwale, Litesh Sulbhewar, Gilles Bailet, and Colin R. McInnes. Towards the commercial development of orbiting reflectors: a technology demonstration roadmap. In *73rd International Astronautical Congress (IAC 2022)*, Paris, France. Paper no. IAC–22–C3.2.x70070.

[12] Russell Bewick, Joan Pau Sanchez, and Colin R. McInnes. Use of orbiting reflectors to decrease the technological challenges of surviving the lunar night. In *62nd International Astronautical Congress (IAC 2011)*, volume 2, pages 1597–1609, Cape Town, South Africa, 2011. IAF. Paper no. IAC-11-A5.1.11.

[13] Drew Gillespie, Andrew Ross Wilson, Donald Martin, Gareth Mitchell, Gianluca Filippi, and Massimiliano Vasile. Comparative analysis of solar power satellite systems to support a moon base. In *71st International Astronautical Congress (IAC 2020)*, Online, 2020. IAF. Paper no. IAC-20,C3,4,2,x59999.

[14] Robert J McKay, Malcolm Macdonald, James Biggs, and Colin McInnes. Survey of highly non-keplerian orbits with low-thrust propulsion. *Journal of Guidance, Control, and Dynamics*, 34(3):645–666, 2011.

[15] Colin R McInnes. *Solar sailing: technology, dynamics and mission applications*. Springer Science & Business Media, 2004.

[16] Daniel J Scheeres. *Orbital motion in strongly perturbed environments: applications to asteroid, comet and planetary satellite orbiters*. Springer, 2016.

[17] B Williams, P Antreasian, E Carranza, C Jackman, J Leonard, D Nelson, B Page, D Stanbridge, D Wibben, Ka Williams, et al. Osiris-rex flight dynamics and navigation design. *Space Science Reviews*, 214(4):1–43, 2018.

[18] Hannah R Goldberg, Özgür Karatekin, Birgit Ritter, Alain Herique, Paolo Tortora, Claudiu Prioroc, Borja Garcia Gutierrez, Paolo Martino, and Ian Carnelli. The Juventas CubeSat in support of ESA's Hera mission to the asteroid Didymos. In *33rd SmallSat Conference*, Logan, Utah, 2019. AIAA/Utah State University.

[19] Colin R McInnes. Mars climate engineering using orbiting solar reflectors. In *Mars*, pages 645–659. Springer, 2009.

[20] FJT Salazar, CR McInnes, and OC Winter. Intervening in earth's climate system through space-based solar reflectors. *Advances in Space Research*, 58(1):17–29, 2016.

[21] John Bookless and Colin McInnes. Dynamics and control of displaced periodic orbits using solar-sail propulsion. *Journal of Guidance, Control, and Dynamics*, 29(3):527–537, 2006.

[22] Robert L Forward. Solar photon thrustor. *Journal of Spacecraft and Rockets*, 27(4):411–416, 1990.

[23] Bernd Dachwald and Patrick Wurm. Mission analysis and performance comparison for an advanced solar photon thruster. *Advances in Space Research*, 48(11):1858–1868, 2011.

[24] Darin C Koblick, Shujing Xu, and Praveen Shankar. Enhancing debris tracking missions in geostationary orbit with advanced solar photon thrusters. *Journal of Spacecraft and Rockets*, 57(3):528–538, 2020.

[25] Paul Fieseler, Kevin R Anderson, and Vaughn Cable. Critical look at the solar photon thruster concept. *Journal of Spacecraft and Rockets*, 52(4):1152–1162, 2015.

[26] Hanspeter Schaub and John L Junkins. *Analytical mechanics of space systems*. American Institute of Aeronautics and Astronautics, 2009.

[27] Chauncey Uphoff. Very fast solar sails. In *International Conference Space Missions and Astrodynamics III*, 1994.

[28] Giovanni Vulpetti, Les Johnson, and Gregory L Matloff. *Solar sails: a novel approach to interplanetary travel*. Springer, 2008.

[29] Kim Eric Drexler. *Design of a high performance solar sail system.* PhD thesis, Massachusetts Institute of Technology, 1979.

[30] René Heller, Michael Hippke, and Pierre Kervella. Optimized trajectories to the nearest stars using lightweight high-velocity photon sails. *The Astronomical Journal*, 154(3):115, 2017.

[31] Robert F Stengel. *Optimal control and estimation*. Courier Corporation, 1994.

[32] Hoyt C Hottel. A simple model for estimating the transmittance of direct solar radiation through clear atmospheres. *Solar energy*, 18(2):129–134, 1976.

[33] Vladimir A Chobotov. *Orbital mechanics*. AIAA, 2002.

[34] M Leipold, E Borg, S Lingner, A Pabsch, R Sachs, and W Seboldt. Mercury orbiter with a solar sail spacecraft. *Acta Astronautica*, 35:635–644, 1995.

[35] Andreas Borggräfe, Jeannette Heiligers, Matteo Ceriotti, and Colin R McInnes. Shape control of slack space reflectors using modulated solar pressure. *Proceedings of the Royal Society A: Mathematical, Physical and Engineering Sciences*, 471(2179):20150119, 2015.

[36] Jiafu Liu and Colin R McInnes. Modulated solar pressure-based surface shape control of paraboloid space reflectors with an off-axis sun-line. *Smart Materials and Structures*, 27(3):035012, 2018.

[37] Artur R Davoyan, Jeremy N Munday, Nelson Tabiryan, Grover A Swartzlander, and Les Johnson. Photonic materials for interstellar solar sailing. *Optica*, 8(5):722–734, 2021.